Supporting Information

CuO nanoplatelets with highly dispersed Ce-doping derived from intercalated layered double hydroxides for a synergistically enhanced oxygen reduction reaction in Al-air batteries

Qingshui Hong, Huimin Lu*, Junren Wang

School of Materials Science and Engineering, Beihang University, XueYuan Road No.37, HaiDian District，Beijing 100191, China

** To whom correspondence should be addressed: lhm0862002@aliyun.com*

Total No. of Pages: 10 (Pages S1-S9).
Total No. of Figures: 4 (Figures S1-S4).
Total No of Tables: 5 (Table S1-S5).
References: 12 (ref S1-S12)

Contents

Supplementary Note

Instrumentation and methods

Characterizations: X-ray diffraction patterns were collected on a Rigaku D/MAX 2000 X-ray generator and diffractometer using a Cu Kα source, with a scan step of 0.02° and a scan range between 3° and 70°. X-ray photoelectron spectra (XPS) were performed on a Thermo escalab 250Xi X-ray photoelectron spectrometer at a pressure of about 2×10^{-9} Pa using Al Kα X-rays as the excitation source. The specific surface area determination was determined by nitrogen physisorption at liquid nitrogen temperature using a Micromeritics Apparatus (Model ASAP2020). The sample morphologies and compositions were investigated on a transmission electron microscopy (TEM, Tecnai G2 F20) equipped with scanning transmission electron microscope (STEM) and energy dispersive X-ray (EDX). The elemental content analysis was conducted on scanning electron microscopy (SEM, CamScan-3400) coupled with energy dispersive X-ray spectroscopy (EDS).

Electrochemical measurements

Al-Air Batteries Test: A two electrode configuration was used for Al-air battery test by pairing catalyst loaded on a carbon fiber paper substrate (GDS2240 with a micro-porous layer, Ballard Power Systems, Inc., 1 cm^2, 275 μm thick, <14 $m\Omega\cdot cm^2$, catalyst loading 0.05 mg) as the air electrode with an Al foil (Alfa Aesar) as the anode in 20 ml of 6 M KOH. The air electrode was prepared using the hot press method. To

fabricate the catalyst layer, the catalysts, carbon black (CB), and 5 wt% polytetrauoro-ethylene (PTFE) emulsion with the mass ratio of 2:2:5 were mixed in appropriate alcohol, and then grinded in an agate mortar to form homogeneous slurry. After the homogeneous slurry turned into paste, it was rolled to the carbon fiber paper substrate until the thickness of this layer was about 0.2 mm and then pressed at 2 MPa using a hot press machine. The thickness of the air electrodes was in the range of 0.3-0.4mm. Finally, the air electrodes were sintered at 350 °C for 1 h at muffle furnace in air atmosphere. Constant current discharges of 35 mA cm^{-2} and dynamic galvanostatic measurements of up to 150 mA cm^{-2} (30 min for every discharge plateau) were carried out on a LAND testing system. The anode utilization (η_A), specific capacity and energy density were calculated using the following formulas:

$\eta_A = It / (\Delta m\ F/9)*100\%$ (1)

Specific capacity = $It / \Delta m$ (2)

Energy density = $EIt / \Delta m$ (3)

Where η_A is the anode utilization (%), I is the discharging current (A), Δm is the weight loss of the anode (g), F is the Faraday constant and t is the discharging time (s); E is the average discharging voltage (V).

Rotating Disk Electrode Tests: The Rotating Disk Electrode (RDE) voltammetry was performed on a MSRX electrode rotator (Pine Instrument) and recorded on a Gamery Reference 3000 electrochemical workstation. A catalyst-modified glassy carbon (GC) electrode (5 mm diameter) was used as the working electrode, and a platinum electrode (2 cm×2 cm square) and an Hg/HgO electrode (0.1 M KOH, 0.164

V *vs* SHE) were used as the counter and reference electrodes, respectively. A 0.1 M KOH solution was used as the electrolyte, which was purged with argon or oxygen for at least 30 min prior to the electrochemical test. The catalyst ink was prepared by dispersing 2 mg Cu-Ce-O catalyst into 1.5 mL ethanol solution containing 50 μL of 5 wt% Nafion (Alfa Aesar, D520 dispersion) by sonication for 30 min. 5 μL of the obtained catalyst ink was loaded on polished GC electrode and dried at room-temperature overnight. Cyclic voltammograms (CVs) were performed from 0.8 to -0.8 V at a scan rate of 50 mV s^{-1}. The linear sweep voltammograms (LSVs) were conducted from 0 to -0.8 V with the scan rate of 5 mV s^{-1}. The Tafel slope was calculated according to Tafel equation as follows:

$$\eta = b \cdot \log(j/j_0) \qquad (4)$$

Where η denotes the overpotential, b denotes the Tafel slope, j denotes the current density, and j_0 denotes the exchange current density. The overpotential was calculated as follows:

$$\eta = E \text{ (vs. Hg/HgO)} - 0.296 \text{ V} \qquad (5)$$

considering the O_2/H_2O equilibrium at 0.296 V vs. Hg/HgO in 0.1 M KOH. The onset potentials were determined based on the beginning of the linear region in Tafel plots. The overall n per oxygen molecule can be calculated from the slopes of K-L plots using the following equation:

$$1/j = 1/j_k + 1/B\omega^{1/2} \qquad (6)$$

$$j_k = nFkC_0 \qquad (7)$$

Where j is the measured current density, j_k is the kinetic current in amperes at a constant potential, ω is the angular velocity of the disk in the radian, k is the electron transfer rate constant and B is the reciprocal of the slope determined from K-L plots based on the Levich equation:

$$B = 0.62nFD_0^{2/3} \nu^{-1/6} C_0 \quad (8)$$

Where n is the total number of electrons transferred during the ORR test, F is the Faraday constant (96 485 C mol^{-1}), D_0 is the diffusion coefficient of O_2 in 0.1 M NaOH (1.9×10^{-5} cm^2 s^{-1}), ν is the kinematic viscosity of the electrolyte (0.01 cm^2 s^{-1}), C_0 is saturation concentration of O_2 in 0.1 M NaOH at 1 atm O_2 pressure (1.2×10^{-6} mol cm^{-3}). For comparison, Commercial Johnson-Matthey 20 wt% Pt/C was measured at the same condition.

Supplementary Figures and Tables

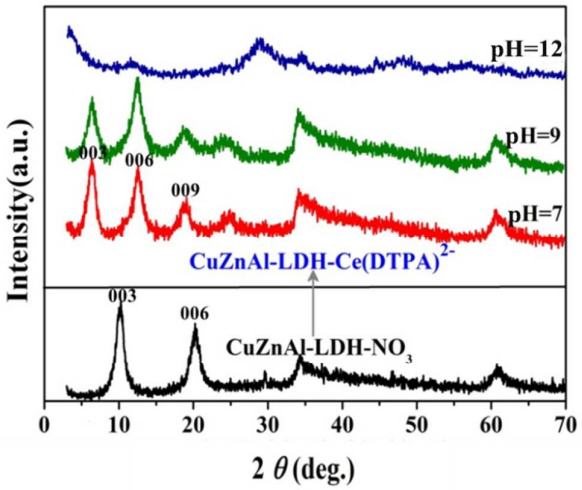

Figure S1. XRD patterns of the CuZnAl-LDHs before and after anion exchange at different pH values.

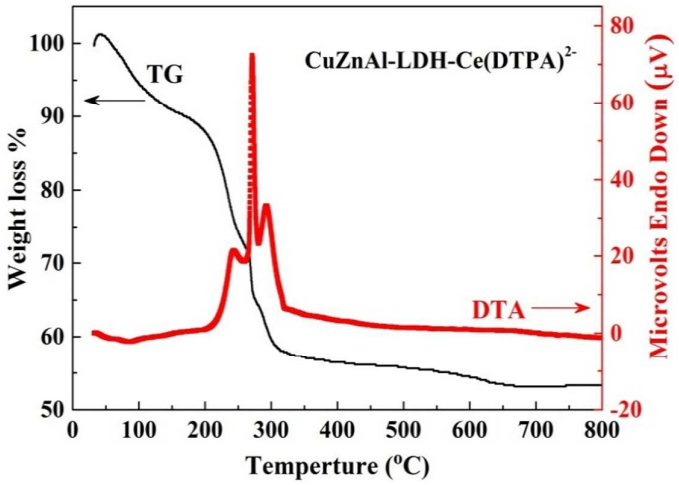

Figure S2. TG/DTA curves of the CuZnAl-LDH-Ce(DTPA)$^{2-}$.

Through careful selections of the anion exchange pH (see Figure S1), we obtained CuZnAl-LDH-Ce(DTPA)$^{2-}$ precursors with well-defined LDH phase at pH = 7. The annealing treatment was performed at 550 °C for 6 h according to the results of TG/DTA curves of the CuZnAl-LDH-Ce(DTPA)$^{2-}$. After 350 °C, almost no change in weight or heat is detected, indicating that the sample is in a relatively stable state (Figure S2).

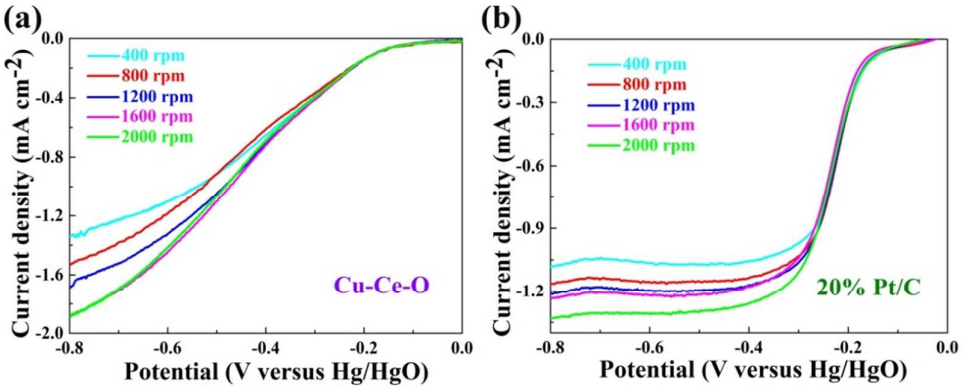

Figure S3. LSV curves at the different rotation rates of (a) the Cu-Ce-O oxide and (b) 20% Pt/C catalysts.

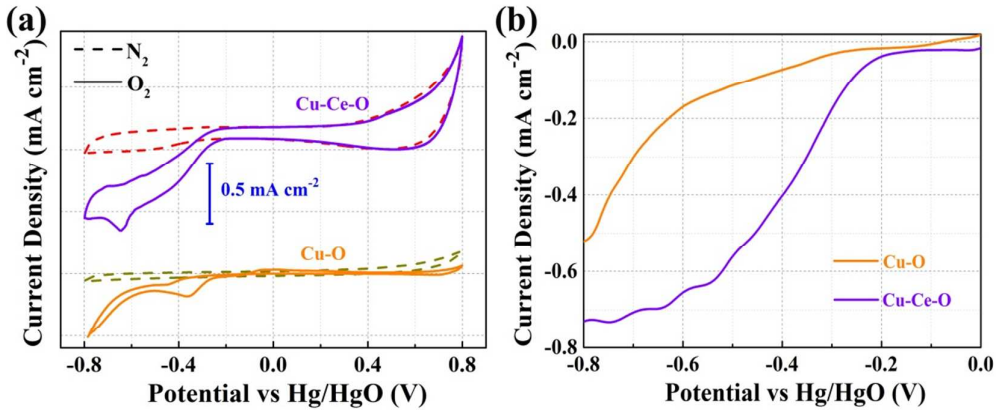

Figure S4. (a) CVs and (b) ORR polarization curves of Cu-Ce-O oxide and Cu-O in (solid lines) O_2- and (dash lines) N_2-saturated 0.1 M KOH.

Table S1. Elemental contents of the Cu-Ce-O oxide determined by XPS spectra.

Sample	Cu 2p (%)	Ce 3d (%)	Zn 2p (%)	Al 2p (%)	C 1s (%)	O 1s (%)
Cu-Ce-O	52.9	6.9	0.5	2.2	2.52	35.07

Table S2. Elemental contents of CuZnAl-LDH-NO_3^--pH, CuZnAl-LDH-Ce$(DTPA)^{2-}$ and their derived calcined products determined by EDS spectra.

Sample	Atom Ratio (%)			
	Cu	Ce	Zn	Al
CuZnAl-LDH-NO_3^--7	15.72	0	20.73	63.55
CuZnAl-LDH-NO_3^--9	13.61	0	21.77	64.62
CuZnAl-LDH-NO_3^--12	6.52	0	26.31	67.17
CuZnAl-LDH-Ce$(DTPA)^{2-}$	14.71	2.35	20.74	62.20
Cu-O	98.61	0	0.51	0.88
Cu-Ce-O	86.87	12.27	0.32	0.54

Table S3. Comparison of the mixed oxides BET surface area from this work and previous literature.

Sample	BET surface area (m^2 g^{-1})	*Ref.*
Cu-O	9.87	This work
Cu-Ce-O	108.53	This work
CuCeO	45	1
CuCe-500-6	47.6	2
CeO_2/CuO	34.7	3

Table S4. A detailed comparison of the Al-air batteries using the Cu-Ce-O oxide electrode and commercial 20% Pt/C electrode.

Cathode material	E_{cell} @ j = 35 mA cm^{-2} (V)	Specific capacity density (mA h g^{-1})	Energy density (W h kg^{-1})	η_A (%)
Cu-Ce-O	1.41	2912.6	4106.8	97.7
20% Pt/C	1.38	2940.9	4058.4	98.9

Table S5. Summary of the ORR catalytic activity of Cu-Ce-O and relevant leading transition metal oxides ORR catalysts reported in recent literatures measured in 0.1 M KOH.

Catalysts	Catalyst loading (μg cm^{-2})	$\Delta E_{\text{onset potential}}$ (V)	Electron transfer number	*Ref.*
Cu-Ce-O	33	-0.02	3.45	This work
$CoFe_2O_4$/3D NS-rGO	156	-0.07	~4.0	4
Cs-MnO_x	280	-0.03	4.05	5
CoO@N/S-CNF	80	-0.09	~4.0	6
MnO_x–CeO_2/KB	80.9	-0.01	~4.0	7
Ag/ $LaMnO_3$ /rGO	317	-0.05	3.91	8
Co@Co_3O_4/NC	210	-0.07	unknown	9
$Co(OH)_2$/CB/N-rGO	100	-0.12	3.3	10
Co@Co_3O_4/BNCNTs-300	710	-0.03	3.85	11
Co@Co_3O_4@C-CM	100	-0.01	3.85	12

($\Delta E_{\text{onset potential}} = E_{\text{onset potential,catalyst}} - E_{\text{onset potential,Pt/C}}$. The more positive $\Delta E_{\text{onset potential}}$ indicates the higher ORR activity)

References

1. Wang, Z. H.; Li, R.; Chen, Q. W., Enhanced activity of CuCeO catalysts for CO oxidation: influence of Cu_2O and the dispersion of Cu_2O, CuO, and CeO_2. *Chemphyschem* **2015,** *16*, 2415-2423.

2. Chang, Z.; Zhao, N.; Liu, J.; Li, F.; Evans, D. G.; Duan, X.; Forano, C.; de Roy, M., Cu-Ce-O mixed oxides from Ce-containing layered double hydroxide precursors: Controllable preparation and catalytic performance. *J. Solid State Chem.* **2011,** *184*, 3232-3239.

3. Xie, Y.; Gao, M. Y.; Zhang, H.; Zeng, S. H.; Zhao, X. Z.; Zhao, Y. H.; Su, H. Q.; Song, J. C.; Li, X. S.; Jia, Q. H., Improvement role of CNTs on catalytic performance in the CeO_2/xCNTs-CuO catalysts. *Int. J. Hydrogen Energy* **2016,** *41*, 21979-21989.

4. Yan, W.; Cao, X.; Tian, J.; Jin, C.; Ke, K.; Yang, R., Nitrogen/sulfur dual-doped 3D reduced graphene oxide networks-supported $CoFe_2O_4$ with enhanced electrocatalytic activities for oxygen reduction and evolution reactions. *Carbon* **2016,** *99*, 195-202.

5. Mosa, I. M.; Biswas, S.; El-Sawy, A. M.; Botu, V.; Guild, C.; Song, W.; Ramprasad, R.; Rusling, J. F.; Suib, S. L., Tunable mesoporous manganese oxide for high performance oxygen reduction and evolution reactions. *J. Mater. Chem. A* **2016,** *4*, 620-631.

6. Liu, T.; Guo, Y.-F.; Yan, Y.-M.; Wang, F.; Deng, C.; Rooney, D.; Sun, K.-N., CoO nanoparticles embedded in three-dimensional nitrogen/sulfur co-doped carbon nanofiber networks as a bifunctional catalyst for oxygen reduction/evolution reactions. *Carbon* **2016,** *106*, 84-92.

7. Chen, J. J.; Zhou, N.; Wang, H. Y.; Peng, Z. G.; Li, H. Y.; Tang, Y. G.; Liu, K., Synergistically enhanced oxygen reduction activity of MnOx-CeO_2/Ketjenblack composites. *Chem. Commun.* **2015,** *51*, 10123-10126.

8. Hu, J.; Liu, Q.; Shi, L.; Shi, Z.; Huang, H., Silver decorated $LaMnO_3$ nanorod/graphene composite electrocatalysts as reversible metal-air battery electrodes. *Appl. Surf. Sci.* **2017,** *402*, 61-69.

9. Aijaz, A.; Masa, J.; Rosler, C.; Xia, W.; Weide, P.; Botz, A. J. R.; Fischer, R. A.; Schuhmann, W.; Muhler, M., Co@Co_3O_4 encapsulated in carbon nanotube-grafted nitrogen-doped carbon polyhedra as an advanced bifunctional oxygen electrode. *Angew. Chem. Int. Edit.* **2016,** *55*, 4087-4091.

10. Zhan, Y.; Du, G. J.; Yang, S. L.; Xu, C. H.; Lu, M. H.; Liu, Z. L.; Lee, J. Y., Development of cobalt hydroxide as a bifunctional catalyst for oxygen electrocatalysis in alkaline solution. *ACS Appl. Mater. Interfaces* **2015,** *7*, 12930-12936.

11. Xiao, J.; Chen, C.; Xi, J.; Xu, Y.; Xiao, F.; Wang, S.; Yang, S., Core-shell Co@Co_3O_4 nanoparticle-embedded bamboo-like nitrogen-doped carbon nanotubes (BNCNTs) as a highly active electrocatalyst for the oxygen reduction reaction. *Nanoscale* **2015,** *7*, 7056-7064.

12. Xia, W.; Zou, R. Q.; An, L.; Xia, D. G.; Guo, S. J., A metal-organic framework route to in situ encapsulation of Co@Co_3O_4@C core@bishell nanoparticles into a highly ordered porous carbon matrix for oxygen reduction. *Energ. Environ. Sci.* **2015,** *8*, 568-576.